Chapter 1

The Method of Fundamental Solutions for Direct Cavity Problems in EIT

D. Borman, D.B. Ingham, T.B. Johansson and D. Lesnic
Department of Applied Mathematics,
University of Leeds, Leeds LS2 9JT, UK
Email: d.j.borman@leeds.ac.uk

Abstract. *The Method of Fundamental Solutions (MFS) is an effective technique for solving linear elliptic partial differential equations, such as the Laplace and Helmholtz equation. It is a form of indirect boundary integral equation method and a technique that uses boundary collocation or boundary fitting. In this paper the MFS is implemented as a technique to initially solve the forward (direct) mathematical problem, where the location of an obstacle within a region of interest is known. In the special issue of the conference proceedings the MFS procedure will be used to solve the inverse problem using a nonlinear constrained minimisation procedure that locates the position of an obstacle within a region of interest based on the boundary Cauchy data.*
Keywords*.MFS, EIT, Laplace's equation, Cavity.*

1.1 Introduction: Electrical Impedance Tomography

Electrical Impedance Tomography (EIT) is a procedure to obtain the spatial properties of the interior of an object from electrostatic measurements taken at its boundary. A typical EIT technique would involve connecting an array of electrodes to the boundary of an object and applying small currents to all or some of the electrodes [Henderson and Webster 1978, Barber and Brown 1984, Borcea 2002]. The resulting electrical potentials can be measured and the process can be repeated for numerous different configurations.

EIT is a non evasive technique and this can be of particular benefit when it is used for medical imaging. The process uses no ionising radiation, therefore it is possible to use the system for continuous monitoring, and it is able to produce thousands of images per second. There is a large resistively contrast (up to 200:1) between a wide variety of tissue types in the body [Geddes and Baker 1967, Faes et al. 1999]. It is also the case that normal tissue types often have significantly different resistance values to that of pathological tissues, such as some tumors and gliomas, enabling these constituents to be monitored using EIT. However, one of the current drawbacks is a low spatial resolution [Boone 2006].

Commonly, a current through a homogeneous object will induce a different electrostatic potential than the same current through a similar object with an enclosed cavity [Hanke and Bruhl 2003]. The electrical potential produced across the object containing the enclosed cavity will depend on the precise location and the electrical properties of the cavity. This implies that it should be possible to use boundary measurements of the potential to detect and locate such cavities [Hanke and Bruhl 2003, Holder 2005].

In mathematical terms, the problem of recovering the conductivity information is a nonlinear inverse problem and is severely ill-posed. It is therefore important to incorporate as much aprori knowledge about the object as possible. To obtain an image with a good spatial resolution, a large number of measured potentials between electrodes are required.

From the point of view of developing a mathematical model to generate the image, the known quantities are the voltages and currents at specific points around the body and the unknowns are the impedances within the body. As outlined in [Boone 2006], at low frequencies, these quantities are related by the Laplace equation:

$$\nabla \cdot (\sigma \nabla \phi) = 0, \tag{1.1}$$

where σ is the conductivity, ϕ is the potential and ∇ is the gradient operator.

In this paper we initially describe the numerical method, namely, the method of fundamental solutions (MFS), for solving direct problems associated to equation (1.1). Following the successful implementation of the direct problem the, inverse EIT problem, which requires detecting a cavity inside an object from a single pair of Cauchy outer boundary data will be investigated in the special issue paper.

1.1.1 MFS background and development

The MFS is a member of a class of boundary-type techniques that involve computations being undertaken with respect to points on the boundary of the region of interest. As such, they do not involve interior points of the region of interest, which is useful in many real world applications. The boundary element methods reduce the dimensionality of the problem and can therefore offer an improved computational efficiency. One of the best known techniques is the Boundary Integral Equation Method (BIEM) and it has been shown that the MFS can be viewed as a form of BIEM [Johnston and Fairweather 1984].

The sources, poles, or singularities, that are needed to construct the base functions are located outside the solution domain and this makes the solution non-singular inside the domain. The expansion coefficients can be determined so that the solution satisfies the boundary conditions with the help of direct collocation. There are a number of techniques for selecting the location of the source points and it has been seen that this selection can have a serious impact on the accuracy.

1.1.2 Developing a function for the potential, ϕ

For simplicity, initially the problem considered will be limited to two dimensions. Let $\phi(P)$ indicate the value of the potential function at any point $P(x, y) \in \overline{D} = D \cup \partial D$, where D is the region occupied by the flow and ∂D is its boundary. If $\sigma = constant$ then ϕ satisfies Laplace's equation

$$\nabla^2 \phi(P) = 0 \text{ for } P \in D. \tag{1.2}$$

In the MFS, an approximate solution for ϕ is sought in the form [Bogomolny 1985]:

$$\phi_N(\underline{C}, \underline{Q}; P) = \frac{1}{2} \sum_{j=1}^{N} C_j ln[(\xi_j - x)^2 + (\eta_j - y)^2], \tag{1.3}$$

where $Q_j(\xi_j, \eta_j)$ are the singularities which are assumed to be located outside $\overline{D}$. The coefficients C_j and the locations of the singularities are chosen to make ϕ_N satisfy the boundary conditions as well as possible.

1.1.3 Imposing boundary conditions

In the first instance, Dirichlet boundary conditions will be used, i.e.

$$\phi(P) = g(P), \quad P \in \partial D, \text{where g is a specified function.} \tag{1.4}$$

If we take $P_i = (x_i, y_i)$ for i=1,2,...,M in (1.3) then

$$g(x_i, y_i) = \phi_N(\underline{C}, \underline{Q}; x_i, y_i) = \frac{1}{2}\sum_{j=1}^{N} C_j ln[(\xi_j - x_i)^2 + (\eta_j - y_i)^2], \text{ i=1,2...,}M. \tag{1.5}$$

In this case, M is the number of points taken on the boundary ∂D and N is the number of singularities taken outside the domain $\overline{D}$. In the case when we have two disjointed boundaries, for example an internal Γ_0 and external Γ_1, as in the case of an annulus, then we can take M_1 points on one boundary and M_2 points on the other boundary. The total number of collocating points will be $M = M_1 + M_2$. In the case of an annulus, it is possible to take singularities both inside the inner circle and outside of the outer circle. In this case, we can take N_1 singularities inside and N_2 singularities outside such that $N = N_1 + N_2$. It is possible to vary the number of points N and M taken to see what effect it has on the accuracy of the results.

1.2 Numerical investigation of 2D annulus

In the primary stages of this research it is advantageous to take problems that have an analytical solution, as these provide a means to test the accuracy of the procedure. For different set ups (e.g. varying the number of boundary points M taken, the number of singularities N taken and the distribution of the singularities, etc.), results can be obtained and the effectiveness of the MFS, in that particular set up, evaluated.

1.2.1 Example 1.1

In this first example we will be using a function for ϕ as

$$\phi(x, y) = x^2 - y^2 = r^2 cos(2\theta) \tag{1.6}$$

which satisfies the Laplace equation (1.2) in a region D of interest taken to be a two-dimensional annulus of internal radius R_0 and external radius R_1, centred at the origin. Singularities will be taken both inside the shape and outside. These will be evenly distributed around circles of radii R_{int} (inside) and R_{ext} (outside), respectively. This is illustrated in figure 1.1 where the circular region is shown containing a circular obstacle.

The points P, distributed around the boundary, are those that we have values of ϕ (given analytically in this example) prescribed through the Dirichlet condition (1.4) as

$$on\ \Gamma_0 : \phi = x^2 - y^2 = R_0^2 cos(2\theta),\ R_0 = 0.5, \tag{1.7}$$

$$on\ \Gamma_1 : \phi = x^2 - y^2 = R_1^2 cos(2\theta),\ R_1 = 1.$$

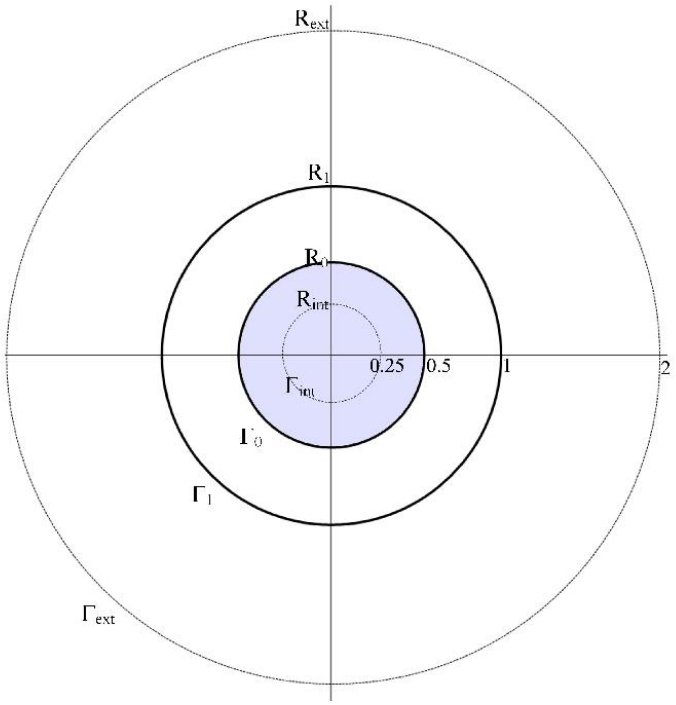

Figure 1.1: Example 1.1 - Circular region with circular obstacle.

1.2.2 Fixing N singularities and M boundary collocation points

It is anticipated that it will be necessary to take a number of singularities both inside and outside the annulus.We choose (ξ_j, η_j) to be uniformly distributed as follows:

(ξ_j, η_j), j= 1,..., N_1 on Γ_{int} =$\{$ r = $R_{int} = 0.25\}$,
(ξ_j, η_j), j= $N_1 + 1$,..., N on Γ_{ext} =$\{$ r = $R_{ext} = 2\}$.

The following expressions distribute the points evenly around the circles of radii R_{int} and R_{ext}, respectively

$$\xi_j = R_{int}cos(\theta_j), \eta_j = R_{int}sin(\theta_j), \text{ for j= 1,...,}N_1, \tag{1.8}$$

where $\theta_j = 2\pi j/N_1$, and

$$\xi_j = R_{ext}cos(\tilde{\theta}_j), \eta_j = R_{ext}sin(\tilde{\theta}_j), \text{ for j= } N_1 + 1, ..., N, \tag{1.9}$$

where $\theta_j = 2\pi(j - N_1)/(N - N_1)$.

In a similar manner as for distributing the singularities evenly around circles, M points on the boundary also need to be identified. Since there are two boundaries, the internal and external, M_1 points were taken on the internal boundary and $M_2 = M - M_1$ points are taken on the external boundary.

We collocate the boundary conditions (1.7) at (x_i, y_i), for $i = \overline{1, M_1}$ on Γ_0, and (x_i, y_i) for $i = \overline{(M_1 + 1), M}$, on Γ_1, namely

$$x_i = R_0cos(\mu_i), y_i = R_0sin(\mu_i), \qquad i = \overline{1, M_1}, \tag{1.10}$$

where $\mu_i = 2\pi i/M_1$ and:

$$x_i = R_1cos(\tilde{\mu}_i), y_i = R_1sin(\tilde{\mu}_i), \qquad i = \overline{M_1 + 1, M}, \tag{1.11}$$

where $\tilde{\mu}_i = 2\pi(i - M_1)/(M - M_1)$.

1.2.3 The MFS procedure development

On developing equation (1.5) it is possible to construct the coefficient vector $\underline{C}$ from a system of linear equations as demonstrated in the following:

$$g_i = g(x_i, y_i) = \frac{1}{2}\sum_{j=1}^{N} C_j ln\{[(\xi_j - x_i)^2 + (\eta_j - y_i)^2]^{\frac{1}{2}}\}, \text{ for } i = 1, ..., M. \tag{1.12}$$

Denoting $\underline{C} = (C_j)_{j=\overline{1,N}}, \underline{g} = (g_i)_{i=\overline{1,M}}$,

$$A(i,j) = ln\{[(\xi_j - x_i)^2 + (\eta_j - y_i)^2]^{\frac{1}{2}}\}, i = \overline{1,M}, j = \overline{1,N}, \tag{1.13}$$

the system of linear equations is generated in the form:

$$A^T A\underline{C} = A^T \underline{g}. \tag{1.14}$$

Since $A^T A$ will always be a square matrix and because $A^T \underline{g}$ will be a column vector of equal size N, the Gauss elimination method can be used to solve the system of linear equations (1.14).

1.2.4 The normal in the radial direction

The normal derivative of ϕ on the boundary is a useful quantity to compare with the analytical solution. Note that for a circular geometry $\frac{\partial\phi}{\partial n} = \frac{\partial\phi}{\partial r}$. To implement this it was necessary to differentiate with respect to r equation (1.5), to obtain an equation for the radial derivative at any point $(rcos\theta, rsin\theta)$ in the domain $\overline{D} = D \cup \partial D$. Converting equation (1.3) to polar co-ordinates and differentiating with respect to r gives:

$$\frac{\partial\phi_N(rcos\theta, rsin\theta)}{\partial r} = \sum_{j=1}^{N} C_j \frac{(rcos\theta - \xi_j)cos\theta + (rsin\theta - \eta_j)sin\theta}{(rcos\theta - \xi_j)^2 + (rsin\theta - \eta_j)^2}. \tag{1.15}$$

1.3 Results of MFS for the annular domain when M=N

Following the development of the program, it was run for $N = M = 4, 8, 16, 32, 64, 128, 256$, where we took $N_1 = N_2 = N/2$ and $M_1 = M_2 = M/2$. In each case, results were obtained for both the values of ϕ and the radial derivative across the annular region. These are plotted at a sufficient density for accurate display of the equipotential lines. At each of the points, the analytical result has also been shown for comparison. Additionally, at each location, the absolute error was calculated by subtracting the analytical result from the MFS result and taking the magnitude. This allowed the error to be plotted in Unimap as a graph of constant errors. Examination of this graph is the most direct technique to see how accurate the results of the MFS are. Figure 1.2(a) shows the MFS results for ϕ when $N = M = 8$ which can be compared with the analytical results. There are small errors in the MFS results that can be seen clearly in figure 1.2(b) which shows the errors between the analytical and MFS results when $N = M = 8$. In this case, it can be seen that the largest errors are approximately of the order of 1/60th of the analytical result.

As the size of $N = M$ increases (more singularities and points on the boundary are taken), the accuracy also improves. Figure 1.2(c) shows the result for $N = M = 32$ where the maximum error is reduced to 1/30,000 of the actual result. This improvement in accuracy is observed to continue as the size of $N = M$ further increases.

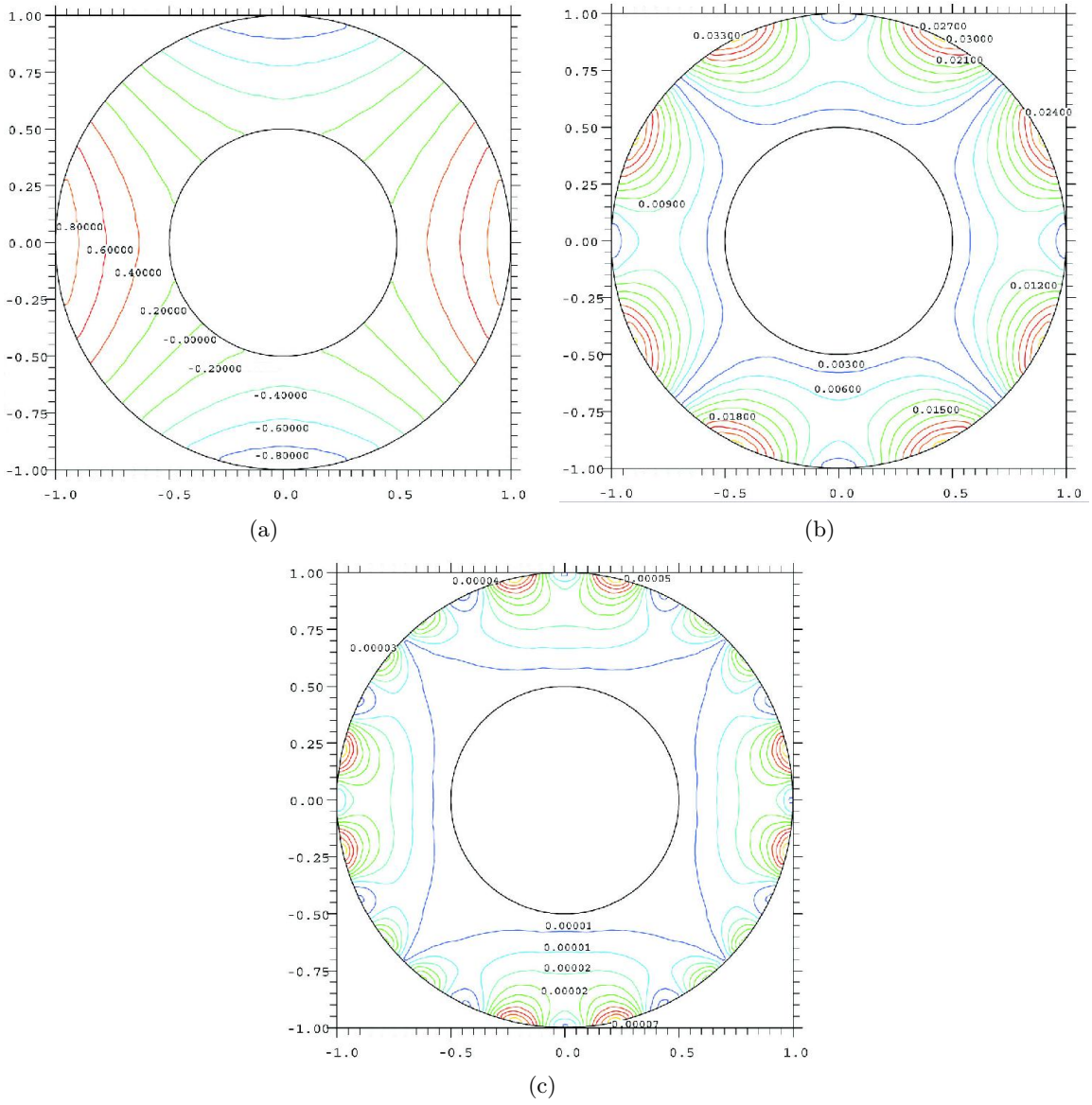

Figure 1.2: (a) MFS results across the annular region when $N = M = 8$. Errors between the MFS and the analytical solution for ϕ across the annular region, (b) when $N = M = 8$ and (c) when $N = M = 32$.

1.3.1 Summary of further results for Example 1.1

A range of investigations were carried out for this example and the results are outlined.

A similar series of results was observed for the radial derivative, namely that the errors also get smaller with increasing matrix sizes (larger values of $N = M$).

A further stage of this work has been to investigate the effect of taking more boundary points than singularities (i.e. taking $M > N$). The results, which are not shown for brevity, identified that this caused relatively small improvements in accuracy for corresponding values of N.

Distributing singularities: The effect of distributing internal and external singularities unevenly was investigated. For the purposes of the experiment, the singularities were still distributed evenly around the internal and external fictious curves Γ_{int} and Γ_{ext}. The refinement

being the ratio of the numbers of internal N_1 and external N_2 singularities taken. This was varied in each test. For the purposes of this stage of the investigation the total number of singularities taken was set at $N = N_1 + N_2 = 16$. Taking odd numbers of singularities was noted to significantly reduce the accuracy of the results. To this end, only the results for even numbers of singularities are considered. Experiments E1 to E9 were run for a range of distributions of internal and external singularities as described in table 1.1. The results are interesting as they

Experiment	E1	E2	E3	E4	E5	E6	E7	E8	E9
Internal-N_1	0	2	4	6	8	10	12	14	16
External-N_2	16	14	12	10	8	6	4	2	0
Max error	0.11	0.038	0.072	0.1	0.033	0.22	0.033	11	7.7
Percentage error	5.5%	1.9%	3.6%	5.0%	1.7%	11%	1.7%	550%	390%

Table 1.1: Summary of results for experiments E1 to E9

suggest that when using the analytical solution (1.6) to define the boundary conditions (1.7) for the annular case, internal singularities are not crucial. This is demonstrated through the observation that, even with no internal singularities, the result is shown to have only a 5.5% error as opposed to the 1.7% in the optimum case. This is still a relatively accurate result and could be improved further through using more external singularities. In the case of no external singularities, the accuracy of the results is not good. When less than four external singularities are taken (experiments E8-E9), the MFS results break down and massive errors are introduced, leaving a meaningless result. The most beneficial distribution appears to be equal numbers of singularities positioned both internally and externally. Similar results were also observed to occur when similar experiments were undertaken to find values of the radial derivative.

Alternative analytical solutions: Two further analytical examples have been investigated, namely that of $\phi(P) = 2xy = r^2 sin(2\theta)$ and that of $\phi(P) = ln(\sqrt{x^2 + y^2}) = ln(r)$. The accuracy of the numerical results for both examples were highly comparable to those in Example 1.1 when equal numbers of singularities are taken on internal and external boundaries. Note that in the later example, which becomes singular at $r = 0$, the location of singularities inside the inner circle was found essential.

Alternative geometries: Following the successful implementation of the technique to an annular domain; the technique was evaluated for other geometries. Investigating a variety of shaped domains further develops the understanding of the MFS procedure. The two domains selected are: (a) Example 1.2, a square obstacle within a circular domain and (b) Example 1.3, two small circular obstacles within a circular domain. The square obstacle is of interest as it contains corners. These will be potential problem areas for the regularity of the solution. The second domain chosen investigates a multiply - connected geometry.

In each case the results again showed similar characteristics to those for the annular problem in Example 1.1. Typical results are illustrated for the case of $N = M = 16$ for which the errors between the analytical (1.6) and MFS results are shown in figures 1.3(a) and 1.3(b) for examples 1.2 and 1.3, respectively. When comparing these results with the results from the annular domain example (with a similar mesh size), it can be clearly observed that the sizes of the errors are highly comparable between the three examples. In each case, the maximum error of 0.033 is distributed around the outer boundary. There are no obvious disruptive errors caused by the corners of the square in Example 1.2.

Implementing Neumann boundary conditions: A further stage of experimentation was undertaken where, instead of using the analytical solution to prescribe the Dirichlet boundary

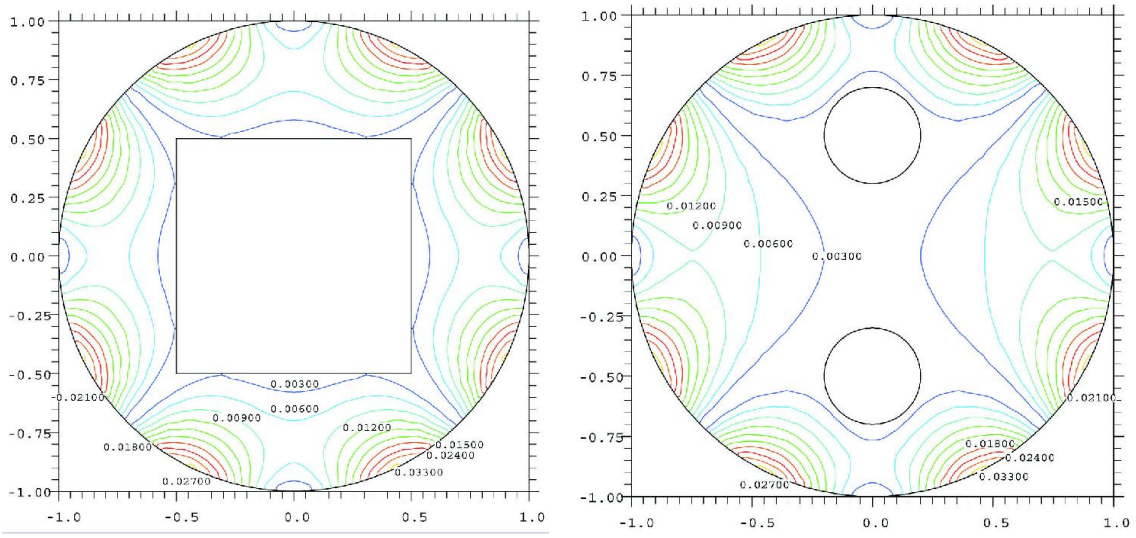

(a) (b)

Figure 1.3: Errors between the MFS and the analytical results for ϕ when $N = M = 16$ across the region between (a) the square obstacle and the outer circle (Example 1.2), and (b) the two circular obstacles and the outer circle (example 1.3).

conditions (1.4), the differential values were calculated at the internal boundary to allow Neumann boundary conditions Γ_0 to be used. The program was re-run using a Neumann boundary condition on Γ_0 and a Dirichlet boundary condition on Γ_1, and the results are highly comparable with those in Example 1.1, produced when the Dirichlet boundary condition only is used.

Example with no analytical solution: A final two-dimensional example is taken where no analytical solution is known. The original annular region of Example 1.1 was used for this investigation. The boundary conditions were fixed such that:

$$\begin{aligned} \text{on } \Gamma_0 &: \phi = 0, \\ \text{on } \Gamma_1 &: \phi = x. \end{aligned}$$

In this example the MFS procedure appears to successfully generate correct solutions. In taking larger mesh sizes and observing the results, it can be clearly seen that values progressively become convergent with larger values of N and M. This indicates strongly that the MFS procedure works successfully in this non analytical case. This example models the physical situation in which Γ_0 is the boundary of a perfectly conducting cavity, i.e. $\sigma = \infty$ inside the inner cavity surrounded by Γ_0.

Developing the MFS technique for three-dimensional domains: Following the successful operation of the MFS approach in two dimensions, the problem was investigated in three-dimensions. To solve the Laplace equation (1.2) in a three-dimensional domain D, it is necessary to adapt the MFS equation (1.3) so that it still satisfies Laplace's equation in three dimensions, namely

$$\phi_N(\underline{C}, \underline{Q}; x, y, z) = \sum_{j=1}^{N} C_j[(\xi_j - x)^2 + (\eta_j - y)^2 + (\zeta_j - z)^2]^{-\frac{1}{2}}, \quad P(x, y, z) \in \overline{D}. \tag{1.16}$$

The first three-dimensional geometry to be considered was that of a spherical cavity enclosed within a spherical region and the second example was that of a cubic region containing a cube shaped obstacle (figures 1.4(a) and 1.4(b), respectively). For brevity, the results for these two

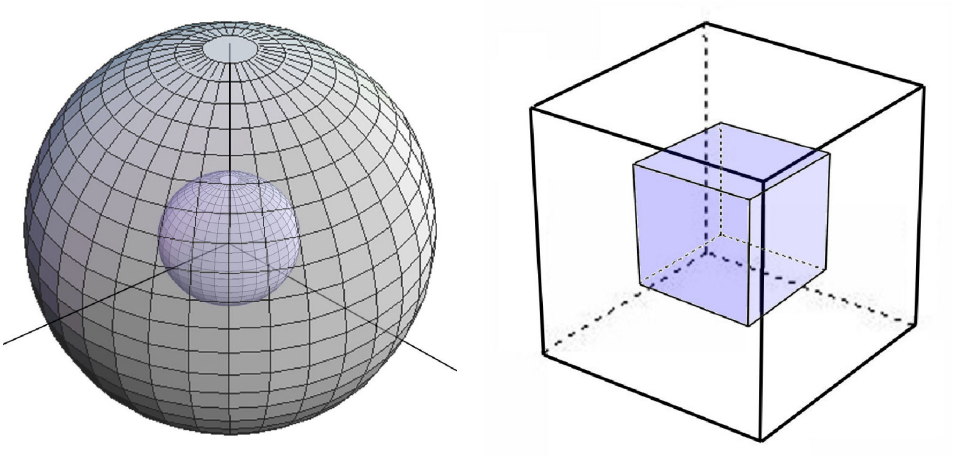

(a) (b)

Figure 1.4: (a) Spherical region of unit radius containing a spherical obstacle of radius 0.5 at the centre, and (b) Cubic region $(-1,1)^3$ containing the cube shaped obstacle $(-0.5,0.5)^3$ at its centre.

examples are summarised. The MFS has been shown to work successfully for both these examples, throughout the region for a range of size obstacles located at various positions within the regions. Figures 1.5(a) and 1.5(b) show the small errors in the results between the analytical solution $\phi(x,y,z) = x^2 + y^2 - 2z^2$ and the MFS results on planes taken through the spherical and cubic domains, respectively, at a height $z = 0.5$. Further reductions in error are observed as the mesh size is increased.

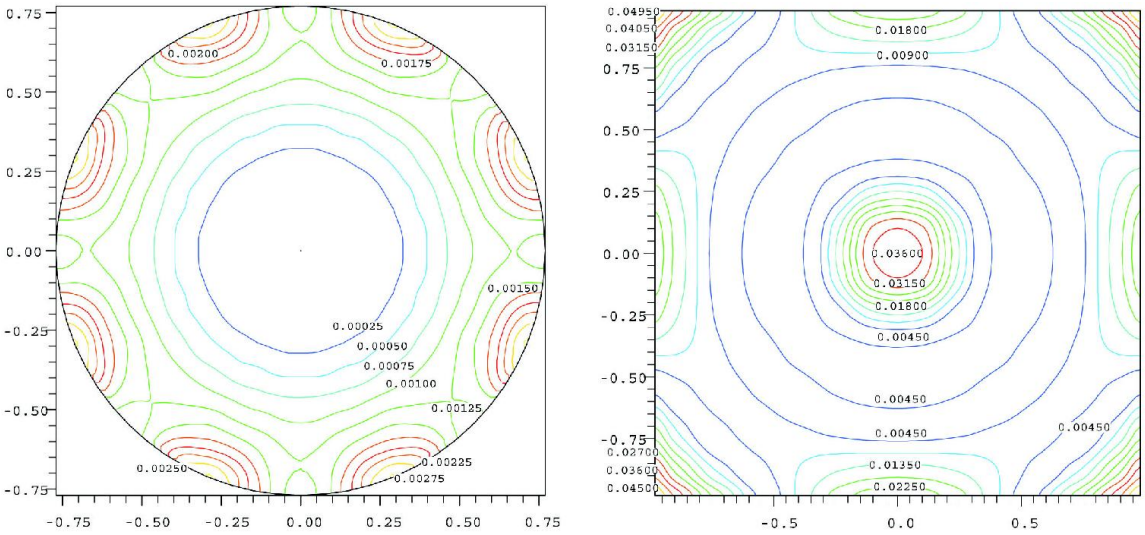

(a) (b)

Figure 1.5: Errors between the MFS and the analytical solution for ϕ across a plane at $z = 0.5$ through (a) spherical region with $M = N = 128$, and (b) cubic region with $M = N = 48$.

1.4 Conclusions

We have successfully demonstrated that the MFS procedure can be used to solve direct problems to a high level of precision in both two- and three-dimensions. Our numerical experiments exhibited robust results for a wide range of complex geometries for problems with and without analytical solutions. Typically, for the two-dimensional MFS technique, to obtain a result that is 99.9% accurate, between 16 and 32 singularities should be taken. In the case of three-dimensional examples, to obtain a similar accuracy then at least 128-256 singularities are required in the case of the spherical region and 192-300 are required in the case of the cubic region. Taking mixed Dirichlet and Neumann boundary conditions has also been shown to be successful when using the MFS technique. The successful application of the MFS procedure in solving the forward problem suggests that it is a robust technique to exploit as a means to solve the inverse problem of identifying the location of an unknown cavity from Cauchy boundary data. The results from further work on the inverse problem will be covered in the special issue paper.

Acknowledgements

Duncan Borman would like to acknowledge the financial support for this work from the Rothschild scheme and the University of Leeds.

References for Chapter 1

[1] Barber, D. and Brown, B. (1984), *Applied tomography*, Phys. E:Sci. Instrum. 17: 723 -733.

[2] Bogomolny, A. (1985), *Fundamental solutions method for elliptic boundary value problems*, SIAM J. Numer. Anal. 22: 644-669.

[3] Boone, K. (2006), *Introduction to Electrical Impedance Tomography*, www.EIT.org.uk, Department of Clinical Neurophysiology, Middlesex Hospital.

[4] J.Borcea, L. (2002), *Electrical impedance tomography*, Inverse Problems 18: R99-R136.

[5] Faes, T., van der Meij, H., de Munck, J. C. and Heethaar, R. M. (1999), *The electric resistivity of human tissues (100Hz-10MHz): a meta-analysis of review studies*, Physiol. Meas. 20:R1-R10.

[6] Fairweather G. and Karageorghis A. (1998), *The method of fundamental solution for elliptic boundary value problems*, Adv. Comput. Math. 9:69-95, 1998.

[7] Geddes, L. and Baker L. (1967), *The specific resistance of biological material- a compendium of data for the biomedical engineer and physiologist*, Med. Biol. Eng. 5: 271-293.

[8] Hanke, M. and Bruhl, M. (2003), *Recent progress in electrical impedance tomography*, Inverse Problems 19: S65-S90.

[9] Henderson, R. and Webster J. (1978), *An impedance camera for spatially specific measurements of the thorax*, IEEE Trans. Biomed. Eng. 25: 250-254.

[10] Holder, D. (2005), *Electrical Impedance Tomography: Methods, History and Applications*, Institute of Physics, Bristol.

[11] Johnston, R. L. and Fairweather, G. (1984), *The method of fundamental solutions for problems in potential flow*, Appl. Math. Modelling 8: 265-270.